



Wake of a Finite-Size Particle in Wall Turbulence Over a Rough Bed

Xing Li^{1,2}, S. Balachandar²(✉), Hyungoo Lee³, and Bofeng Bai¹(✉)

¹ State Key Laboratory of Multiphase Flow in Power Engineering, School of Chemical Engineering and Technology, Xi'an Jiaotong University, Xi'an 710049, China
bfbai@mail.xjtu.edu.cn

² Mechanical & Aerospace Engineering, University of Florida, Gainesville, FL 32608, USA
bala1s@ufl.edu

³ Power Reactor Development Division, Korea Atomic Energy Research Institute, Daedeok-Daero 989, Yuseong-Gu, Daejeon 305–353, Republic of Korea

Abstract. For finite-size particles in turbulence, the particle's wake causes an additional force on the particle, alters the ambient turbulence and thus changes the properties of the two-phase flow. The mechanism of the interaction between the wake and turbulence, is still ambiguous. Here, we performed fully resolved direct numerical simulations with an immersed boundary method and investigated the wake of a stationary finite-size particle in wall turbulence over a rough bed. We focused on the time-dependent features of the wake, and studied the effect of the ambient turbulence on the wake and the turbulence modulation by the wake. Results show that there exists a strong correlation between the wake and the oncoming turbulent flow, which is beneficial for the precise prediction of the wake-induced force on the particle and the turbulence modulation by the wake. Turbulence augmentation is observed far downstream, while turbulence attenuation region lies near the sphere and the wall where viscous effect is dominant. We also found the effect of roughness is prominent in the near-wall region and is weakened far from the wall. In addition, the vortex shedding happens on only one side of the sphere, and the Strouhal number based on the particle center velocity is around 0.262, about twice that in an unbounded flow. The mechanisms we revealed here provide a basis for building the model of the wake-induced force on a finite-size particle and the turbulence modulation by the particle's wake.

Keywords: Particle Wake · Wall Turbulence · Turbulence Modulation

1 Introduction

Finite-size particles, which are comparable to or larger than the Kolmogorov microscale of ambient turbulence, are usually encountered in natural and industrial applications, such as the seabed, aero-engines, fluidized beds, etc. The particle Reynolds number Re_p of a finite-size particle is usually larger than unity and even of the order of $Re_p \sim 100$ or above. In this case, the wake oscillation or vortex shedding of the finite-size particle can induce a non-negligible force on the particle as well as modulate the downstream

turbulence. The wake is an important aspect of dispersed multiphase flows and can be the main factor in deciding the qualitative and quantitative behavior of multiphase systems [1]. For example, in case of fuel droplets in engines and large particles or bubbles in chemical equipment, their performance can be profoundly affected by the particle wakes.

The problem of the wake of a particle in laminar flows has been widely investigated and has formed the basis of analyzing the more complex situation of particle-laden turbulence [2–9]. Generally, the wake evolves from the axisymmetric stationary state to a planar-symmetric double-threaded stationary state and then to a periodic vortex shedding state as the particle Reynolds number increases, and finally towards chaos. Specifically, for a particle in a uniform flow, the wake maintains the stationary axisymmetric state up to $Re_p \approx 212$. Then, the first bifurcation occurs and leads to a stationary state that is no longer axisymmetric but planar symmetric. A second bifurcation, which is a Hopf bifurcation, occurs at $Re_p \approx 273$ and leads to a periodic oscillatory state, and the wake still preserves planar symmetry. The Strouhal number of the periodic oscillation is about 0.127. As the particle Reynolds number grows to $Re_p \approx 285$, the wake oscillation evolves into the vortex shedding. A tertiary Hopf bifurcation occurs at $Re_p \approx 320$, leading to a secondary shedding frequency that is about three times smaller than the primary one. Beyond $Re_p \approx 355$, the wake becomes fully three-dimensional and chaotic [5]. Recently, 3D vortex structures of the sphere wake have been measured via the tomo-PIV method, and different structures were observed in the cases of a stationary and moving sphere [10, 11]. A numerical research was also conducted to investigate the stability and sensitivity of the secondary bifurcation in the sphere wake [12]. Particle wake dynamics at higher Reynolds numbers have also been widely investigated [13–17]. Recently, David et al. investigated the wake of a sphere with a rough surface, and found that the roughness lowers the critical Re_p for the clear, temporally averaged recirculating wake to disappear [18].

In wall-bounded laminar flows, the evolution of the particle wake follows a similar path. The differences lie in the loss of the axisymmetry, which influences the critical Reynolds numbers of the Hopf bifurcations and the structure of the wake. Zeng et al. [19] reported an asymmetric double-threaded wake at a lower critical Reynolds number than that in the unbounded case due to the presence of the nearby wall. Zeng et al. [20] extended this research to examine gap ratio down to 0.005 sphere diameter, where the particle is practically sitting on the bottom wall. Stewart et al. [21] examined the wake of a rolling sphere near a wall, and they found that the critical Reynolds number for transition to the unsteady state depends on the rotation rate, and it is much lower than the critical Reynolds number in the unbounded case. Besides, the Strouhal number of vortex shedding is around 0.12, slightly lower than that in the unbounded case. Rao et al. [22] found the wake of a rolling sphere near a wall to become unsteady at $Re_p \approx 139$, and a lateral oscillation occurs at $Re_p \approx 192$, whose frequency is (3/7)th of the primary shedding frequency.

In turbulence, the wake is prominently influenced by the oncoming turbulent disturbance and is chaotic, unlike its counterpart in a laminar flow which is regular and symmetric. In a turbulent flow, the interaction between the particle wake and the ambient flow is much more complicated. First, because the oncoming flow is turbulent, the onset of wake unsteadiness occurs earlier [23, 24]. Second, the turbulence influences the

wake-induced force on a particle. The oscillating wake or the vortex shedding induces an additional fluctuating force on the particle and changes the particle trajectory. The wake has been shown to enhance the hydrodynamic force fluctuation on a stationary finite-size particle in a uniform turbulent flow [24] and in a wall-bounded turbulent flow [25]. Third, the particle wake modulates the ambient turbulence. Turbulence augmentation usually occurs due to the enhanced velocity fluctuation induced by the unsteady wake [26]. Wu and Faeth [27] experimentally investigated the interaction between the particle wake and the turbulent pipe flow, suggesting that the turbulent wakes behave like self-preserving laminar wakes. Zeng et al. [28] studied the wake response of a stationary finite-size particle in a turbulent channel flow, revealing that the total kinetic energy is reduced in the wake, but the turbulent kinetic energy (TKE) is enhanced due to vortex shedding and wake oscillation. In addition, an enhancement of the wall shear stress was also noticed below the particle. Naso and Properetti [29] investigated the interaction between a fixed sphere and isotropic turbulence and observed that the particle has a profound influence on the turbulence, affecting a region that extends more than 10 times farther downstream than the viscous layer. Cisse et al. [30] investigated the interaction between a large particle and a homogeneous turbulent flow, finding that the particle calms turbulent fluctuations in its wake up to distances of the order of its diameter, probably due to the lower particle Reynolds number ($Re_p = 27 \sim 126$). Recently, van Hout et al. [31] experimentally studied the wake of a stationary sphere in a turbulent boundary layer using time-resolved tomo-PIV, and 3D hairpin-like structures were observed to shed with their “heads” tilted away from the wall, which was believed to cause a negative lift force. Besides, statistics of the wall turbulence modulated by the sphere were also analyzed.

Unlike its apparent counterpart in laminar flows, the natural vortex shedding frequency in a turbulent flow is hidden in turbulent fluctuations [24, 30]. Numerical [25] and experimental [31] results show that the Strouhal number of vortex shedding behind a finite-size particle in wall turbulence is lower than that in a uniform flow, except when the particle is very close to the wall [31].

For the case of many particles, the interaction between particle wakes and ambient turbulence is even more complex. The research of Xu & Bodenschatz [32] indicates that preferential accumulation of finite-size particles can possibly be affected by their wake interaction. Bellani [33] compared the turbulence modulation of spherical and ellipsoid particles and conjectured that the lower reduction in TKE by ellipsoids than the spheres is due to the more energetic wakes produced by ellipsoids. It was also noticed that the wake behind falling elliptical particles due to gravity enhances the TKE production [34]. Yu et al. [35] investigated the statistics of finite-size particles in turbulent channel flows and found the velocity fluctuations in the vicinity of the particle are dissipated more than generated by the presence of the wake. In general, the mechanism of interaction between the particle wakes and ambient turbulence is far from clear.

To our knowledge, the interaction between the wake of a finite-size particle and wall turbulence over a rough bed has not been investigated. The interaction mechanism between a finite-size particle and the ambient turbulence is still ambiguous. How the wake reacts to the oncoming turbulent disturbance is still unclear. In our previously published paper (Li et al., *Phys. Rev. Fluids*, 2019), we conducted an investigation on the finite-size particle over a rough bed. The previous work is focused on the drag and lift force on the

particle, while the current research is focused on the wake characteristics. The objective of the current research is to investigate the interaction between the wake of a stationary finite-size particle and the wall turbulence over a rough bed at $Re_p = 99 \sim 310$, with special emphasis on the time-dependent features of the wake. In Sect. 2, the direct numerical simulation method is introduced. In Sect. 3, the vortex structures behind the particle are analyzed. In Sect. 4, we analyze the turbulence modulation by the wake by examining the time-averaged statistics of the wake. In Sect. 5, time-dependent features of the turbulence\wake interaction are examined, and the correlation between the wake and the oncoming flow is thoroughly discussed. In Sect. 6, the correlation between the wake and the oncoming flow, the turbulence modulation and the Strouhal number of the natural vortex shedding are discussed.

2 Problem Description and Numerical Method

2.1 Problem Description

The set-up of the flow is similar to the one considered in Li et al. [36]. We consider a fully developed open channel flow. The flow is characterized by the friction Reynolds number $Re_\tau = H_* u_{*\tau} / \nu_*$, in which H_* is the channel height and $u_{*\tau}$ is the friction velocity, which are also the length and velocity scales. The time and pressure scales are $H_* / u_{*\tau}$ and $\rho_* u_{*\tau}^2$, respectively, in which ρ_* is the density of the fluid. The friction Reynolds number is $Re_\tau = 180$. The rough bed consists of hemispheres of diameter $d_* = 0.1H_*$, which is shown in Fig. 1. So, in the non-dimensional form, the diameter of the hemispheres is $d = 0.1$. In wall units, the diameter of the particle and the distance from the wall are defined as $d^+ = d_* u_{*\tau} / \nu_*$ and $y_p^+ = y_{p*} u_{*\tau} / \nu_*$, respectively. In this research, we investigate an idealized rough bed which is made up of a single layer of monodispersed spheres. The hemispheres are located on the bottom wall of the channel and their centers are at the “base level”, as shown in Fig. 1. The hemispheres are closely packed. To save on computational cost, the bottom wall of the computational domain is not totally covered with hemispheres, and there are only seven rows and ten columns ($C10 \times R7$) of hemispheres (see Fig. 2). It was shown in [36] that this configuration provides a good representation of the rough bed. The flow is fully adjusted to the rough bed after five rows.

As shown in Fig. 1, the “reference particle” we study is located above the rough bed and is stationary. The gap (δ) between the particle and the rough bed is crucial. Several definitions are proposed by Lee and Balachandar [37], and we choose the definition where the “bed level” is the lowest possible position for a particle sitting on the rough bed (i.e. corresponds to $\delta = 0$). In this case, the location of bed level is at $0.3165d$, i.e. $h_{BL} = 0.3165d$. The particle above the bed has the same diameter as the hemispheres. In the research, three vertical locations of the particle center, which are $\delta = 0.0d$, $\delta = d/3$ and $\delta = 1.0d$ ($y_p^+ = 14.7$, $y_p^+ = 20.7$, and $y_p^+ = 32.7$ in wall units) are investigated.

The instantaneous particle Reynolds number $Re_p = u_*(y_{*p})d_*/\nu_* = u^+(y_p^+)d^+$. As the oncoming flow seen by the particle is fluctuating with time, Re_p also varies. For the particle sitting on the bed, the Re_p ranges from 99 to 218. For the other two cases,

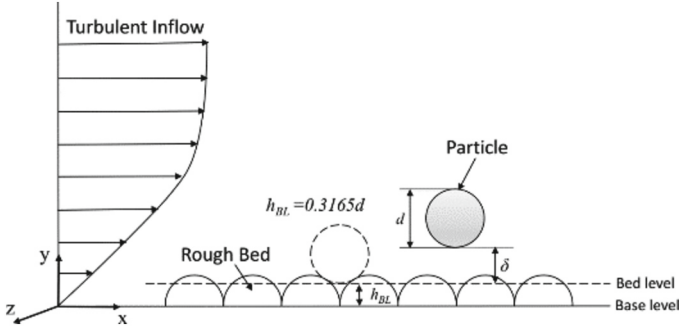


Fig. 1. Schematic of a particle over a rough bed made of hemispheres in a wall-bounded turbulent flow.

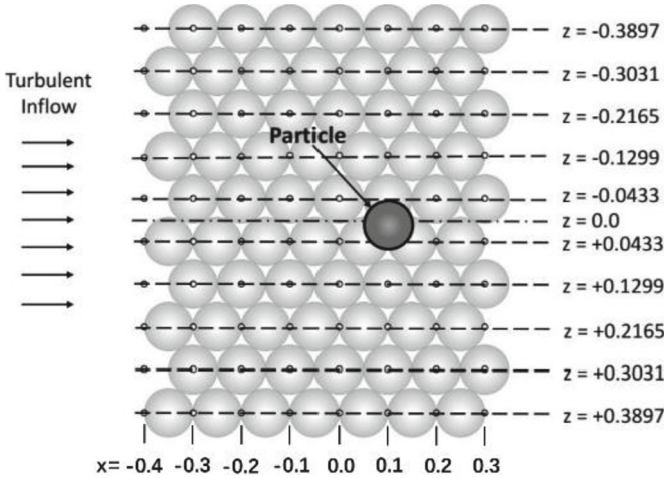


Fig. 2. Top view of the arrangement of the rough bed and the particle.

the oncoming velocity is larger, and the ranges of Re_p are 157 ~ 280 and 174 ~ 310, respectively.

On the bottom boundary of the computational domain, no-slip condition is employed. On the top boundary we enforce free-slip for the streamwise and spanwise velocities and no-penetration for the vertical velocity. In the spanwise direction, periodic boundary conditions are employed. A fully developed turbulent open channel flow is introduced from the inlet of the computational domain in the same way used by Li et al. [36]. In this method, two simulations are performed simultaneously. A typical fully-developed turbulent open channel flow simulation at $Re_\tau = 180$ with periodic boundary conditions employed along the streamwise direction with the bottom wall being smooth is conducted first. The second simulation is the inflow-outflow open channel flow simulation with a rough bed at the bottom and a particle placed above the rough bed, which is described above. The two simulation setups are such that the computational domain of the first simulation has the same wall-normal and spanwise lengths as the second one, and the

outflow velocity of the first simulation is exactly applied as the inlet velocity of the second simulation. In this way, a huge amount of computational cost is saved due to the far less grid points in the first simulation.

2.2 Numerical Methodology

The dimensionless continuity and Navier-Stokes equations for incompressible flow can be written as:

$$\nabla \cdot \mathbf{u} = 0, \quad (1)$$

$$\frac{\partial \mathbf{u}}{\partial t} + \mathbf{u} \cdot \nabla \mathbf{u} = -\nabla p + \frac{1}{Re_\tau} \nabla^2 \mathbf{u} + \mathbf{f}, \quad (2)$$

where Re_τ is the frictional Reynolds number. A finite volume method on a collocated Cartesian grid system is used. For the space discretization, the second-order central difference scheme is employed. For the time advancement, a fractional-step method is used. The nonlinear advection term is discretized explicitly with the second-order Adams-Bashforth scheme, and the diffusion term is treated implicitly with the Crank-Nicolson scheme.

An immersed boundary method is used to resolve the flow around the particle and to capture flow details of all scales [38]. Multilayers of Lagrangian markers are placed within the particle and the hemispheres in order to enhance the accuracy. 20 spherical layers are used and the total number of Lagrangian markers in the particle is 36077. No-slip and no-penetration conditions are employed on the surface of the particle and the hemispheres.

In the first simulation, the extent of the computational domain in non-dimensional terms is $[0, 4\pi] \times [0, 1.0] \times [-4\pi/3, 4\pi/3]$ along the streamwise, wall-normal and spanwise directions, respectively, and the resolution is $257 \times 129 \times 129$. The grid is uniform in the streamwise and spanwise directions and is non-uniform in the wall-normal direction. In the second simulation, the extent is $[-1.0, 1.0] \times [0, 1.0] \times [-4\pi/3, 4\pi/3]$ along the three directions, and the resolution is $481 \times 161 \times 481$. We employed a finer uniform grid in the extent of $[-0.45, 0.4] \times [0, 0.25] \times [-0.44, 0.44]$ along the streamwise, wall-normal and spanwise directions, respectively in order to resolve the flow around the particle and the rough bed more precisely. In this region, the grid sizes along three directions are the same and it is $d/40$. The validity of the domain size and grid resolution are stated in [36, 39, 40].

3 Vortex Structure of the Wake

The three-dimensional vortex structure around the particle in the three cases studied are shown in Fig. 3. It is noticed that the fluid rolls up above each hemisphere composing the rough bed. The sphere above the rough bed, which has the same radius as the hemispheres, is covered by the vortex structure. In Fig. 3(a), the particle Reynolds number is relatively low, ranging from 99 to 218. So no obvious threaded wake is observed behind the sphere.

However, in Fig. 3(b), a double-threaded wake starts forming behind the particle as the particle Reynolds number increases to the range of 157 to 280, which is due to the increase of the particle-to-wall distance. Though the double-threaded wake interferes with the turbulent structures of the oncoming flow, it is still clearly observed. In Fig. 3(c) the threaded wake becomes much more obvious as the particle-to-wall distance increases further. The particle Reynolds number in this case rises to the range of 174 to 310.

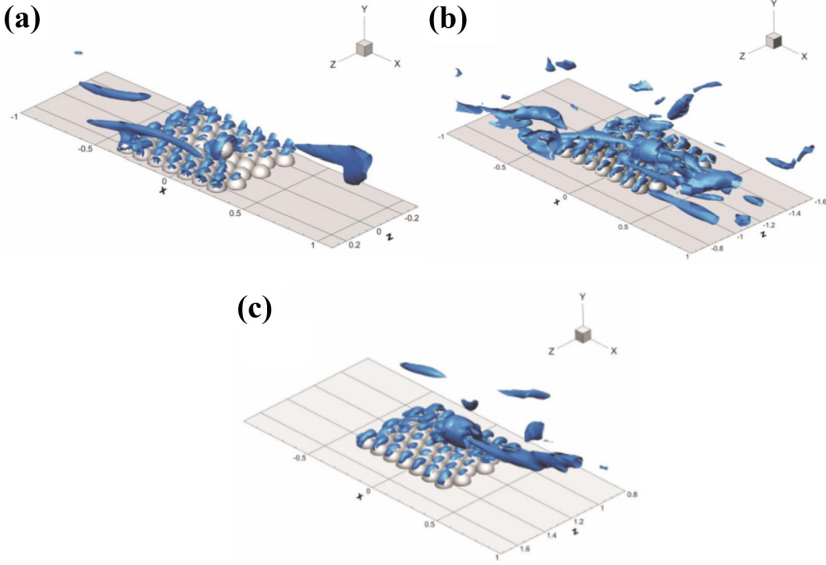


Fig. 3. Three-dimensional nature of the turbulent flow over the rough bed and around the sphere. (a) $\delta^+/d^+ = 0.0$; (b) $\delta^+/d^+ = 1/3$; (c) $\delta^+/d^+ = 1.0$. The vortex structures are shown by the iso-surface of the swirling strength $\lambda_{ci} = 30$.

In order to examine the unsteady features of the wake, streamlines around each sphere at different time instants are shown in Fig. 4, 5, and 6, respectively. Figure 4 shows the evolution of a vortex behind the sphere sitting on the bed. The most notable phenomenon is the asymmetry of the flow field around the sphere due to the presence of the wall, which resembles the flow features of the particle in a laminar shear layer investigated by Zeng et al. [20]. Another notable feature is the unsteady evolution of the vortices. A vortex emerges near the particle centered around $x = 0.21$ (see Fig. 4a). Then, it grows larger, moves downstream at the same time and is centered at $x = 0.41$ in Fig. 4b. Finally, it migrates downstream to the position $x = 0.8$ and towards the wall, which is shown in Fig. 4c. At the same time, the size of the vortex is shrinking. Figure 4 documents the process of vortex shedding in the present case. It is noticed in Fig. 4c that another vortex forms centered at around $x = 0.4$, which implies that successive vortices form and shed behind the sphere.

For the sphere of $\delta^+/d^+ = 1/3$, the flow is still highly asymmetric and the vortex behind the sphere changes over time, though no obvious shedding process is observed. This does not mean the shedding does not exist, but it is affected by the faster moving

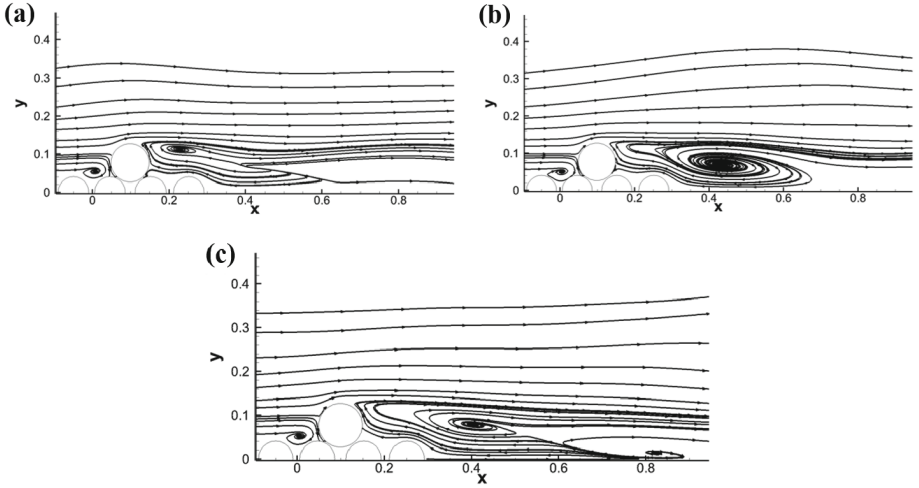


Fig. 4. Streamlines around the sphere of $\delta^+/d^+ = 0.0$. Shown is the x-y plane (side view) through the particle center. (a) $t^+ = 60.66$; (b) $t^+ = 68.22$; (c) $t^+ = 99.54$.

fluid of larger velocity compared with the case of $\delta^+/d^+ = 0.0$. This phenomenon is more noticeable in the case of $\delta^+/d^+ = 1.0$, which is shown in Fig. 6. It can be observed in Fig. 6 that the flow is much less asymmetric than the other two cases due to the enhancement of the particle-to-wall distance. A standing vortex exists at the lower part of the wake near the sphere throughout the whole period. The vortices at the higher part of the wake are shedding vortices that form and migrate downstream successively. It should be noticed that Fig. 6 shows that the shed vortices disappear quickly. The reason is that the turbulent fluctuation deforms or breaks the vortices during the shedding process, making the shedding happen much earlier.

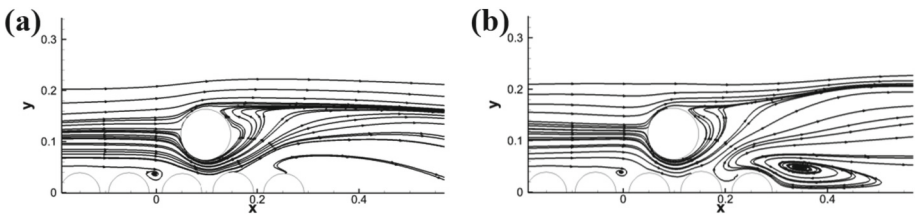


Fig. 5. Streamlines around the sphere of $\delta^+/d^+ = 1/3$. Shown is the x-y plane (side view) through the particle center. (a) $t^+ = 15.318$; (b) $t^+ = 31.518$.

In laminar flows, the threaded wake oscillates or sheds regularly. However, in turbulent flows, the oscillation or shedding process is profoundly affected by the oncoming turbulence. Figure 7 shows the contours of the vorticity magnitude on the x-z plane through the particle center at $y_p^+ = 32.7$ (i.e. the third case). Two oncoming fluctuations are analyzed here. It is noticed when the fluctuation marked by the black circle is passing the sphere, the wake oscillates downward. While the fluctuation marked by the red circle

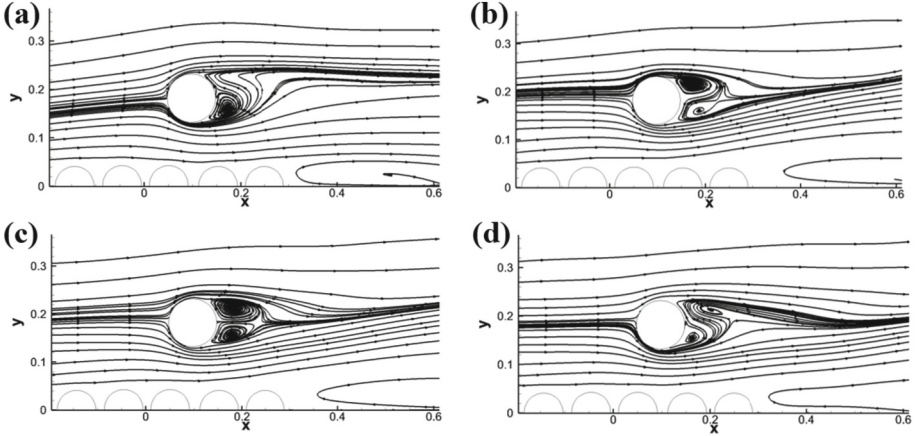


Fig. 6. Streamlines around the sphere of $\delta^+/d^+ = 1.0$. Shown is the x-y plane (side view) through the particle center. (a) $t^+ = 18.558$; (b) $t^+ = 29.358$; (c) $t^+ = 30.438$; (d) $t^+ = 32.598$.

acts on the sphere, the wake oscillates to the opposite direction. Therefore, in this case, the direction of oscillation of the sphere wake is dominated by the oncoming fluctuation, and the self-induced natural shedding frequency is overwhelmed.

4 Turbulence Modulation by the Wake

In this section, time-averaged statistics in the streamwise, wall-normal and spanwise directions of three cases are analyzed. The modulation of wall turbulence by the wake is of the most importance, thus the root mean square velocities and turbulent kinetic energy are investigated.

4.1 Root Mean Square Velocities and Turbulent Kinetic Energy

The r.m.s. velocities and the turbulent kinetic energy for the case of $\delta^+/d^+ = 0.0$ is shown in Fig. 8. It is noticed that behind the sphere, as shown Fig. 8a, the streamwise r.m.s. velocity near it is quite low at $x = 0.2$ ($1.0d$ behind the sphere). The low streamwise r.m.s. velocity region extends to the wall. Above the sphere, the streamwise r.m.s. velocity is high, but it is limited in a thin region. This region expands as the flow moves downstream, which is caused by the vortex shedding behind the sphere. The r.m.s. velocity becomes much higher far downstream, which does not even reach its highest value at the outlet of the computational domain. It indicates that in the moderate particle Reynolds range, the turbulence modulation by the particle wake is definitely not restricted in the area near it. We can notice the obvious turbulence augmentation extends well more than $10.0d$ behind the particle. The contour of the turbulent kinetic energy in Fig. 8(d) indicates the same.

For the wall-normal and spanwise directions, the fluctuation is inhibited near the sphere, but unlike the streamwise fluctuation, the other two components are not augmented far downstream. Their variation is primarily in the wall-normal direction, and

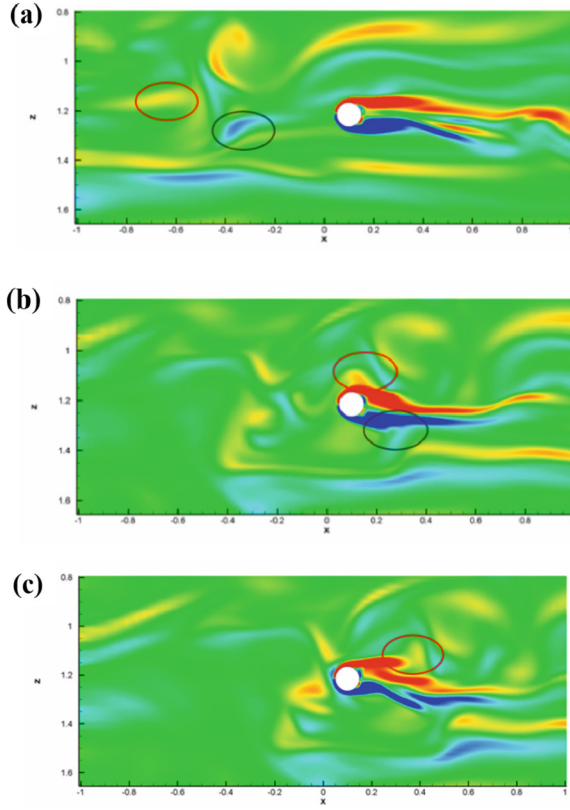


Fig. 7. Contours of vorticity magnitude on the x - z plane through the particle center ($y_p^+ = 32.7$). $\delta^+/d^+ = 1.0$. (a), (b) and (c) show contours of different time instants. Red and black circles mark two different oncoming fluctuations acting on the sphere and its wake.

the similar behavior for both upstream and downstream of the particle suggests a weaker influence of the particle. Only at $x = 0.9$, the wall-normal turbulent kinetic energy starts being augmented, but only by a little. The spanwise turbulent kinetic energy is attenuated near the sphere, but it is not augmented downstream.

As the distance between the sphere and the wall increases to $\delta^+/d^+ = 1/3$, the streamwise turbulent kinetic energy (or r.m.s. velocity) is no longer augmented, as shown in Fig. 9a. The fluctuation is inhibited near the sphere. However, the intensity of the fluctuation does not rise higher than that in the oncoming flow. The highest r.m.s. velocity in the wake is still a little lower than that in the oncoming flow. Turbulence augmentation in the wall-normal and spanwise directions is observed, as shown in Fig. 9b and 9c. The augmentation starts at about $x = 0.7$ and $x = 0.5$ for the wall-normal and spanwise direction, respectively.

For $\delta^+/d^+ = 1.0$, the turbulence augmentation region is much closer to the sphere due to the higher oncoming velocity. In Fig. 10a and 10d, we can see that the turbulent attenuation region still exists near the sphere. Because of the higher particle Reynolds

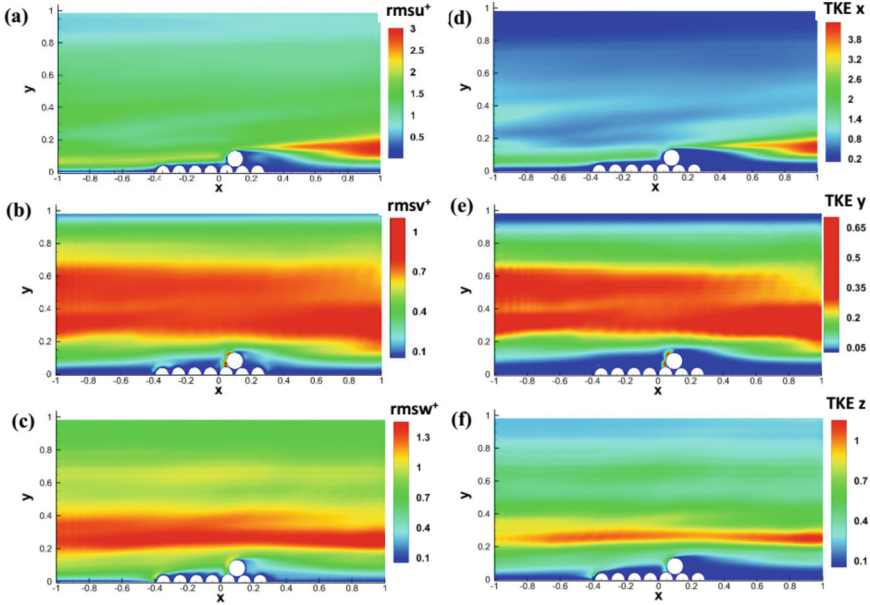


Fig. 8. Root mean square velocities (a-c) and turbulent kinetic energy in three directions (d-f). $\delta^+/d^+ = 0.0$.

number, the vortex shedding becomes stronger, and the region of turbulence augmentation in the streamwise direction locates above the attenuation region and close to the sphere, and it expands to a larger area downstream. In addition, the turbulence attenuation starts decaying at about $x = 0.7 \sim 0.8$, indicating that earlier turbulence attenuation also decays earlier. Similar phenomenon exists in the wall-normal and spanwise direction. The regions of turbulence attenuation locate in the range of about $x = 0.2 \sim 0.6$, much closer to the sphere compared to the cases of $\delta^+/d^+ = 0.0$ and $\delta^+/d^+ = 1/3$. In addition, the magnitude of augmentation is also larger.

4.2 Total Kinetic Energy

The total turbulent kinetic energy is shown in Fig. 11. As the total turbulent kinetic energy is mainly contributed by the streamwise turbulent kinetic energy, for the cases of $\delta^+/d^+ = 0.0$ and $\delta^+/d^+ = 1.0$, turbulence augmentation is observed behind the sphere. But for the case of $\delta^+/d^+ = 1/3$, turbulence augmentation is not noticed in the wake. It should be noted that the regions of turbulence augmentation are different for the cases of $\delta^+/d^+ = 0.0$ and $\delta^+/d^+ = 1.0$. In the former case, this region locates far downstream behind the sphere due to the relatively lower particle Reynolds number; while the region in the latter case is much closer to the sphere, and also decays faster.

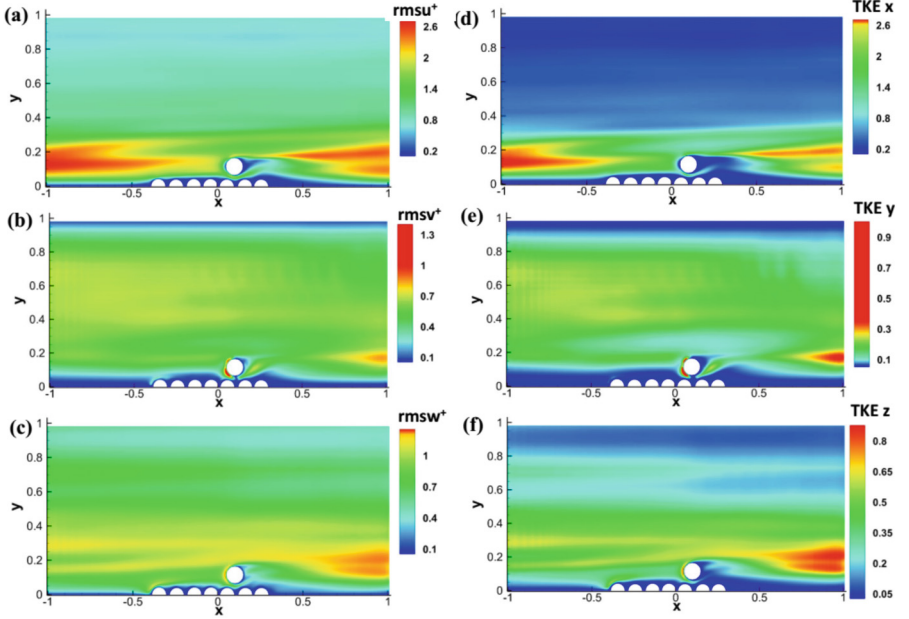


Fig. 9. Root mean square velocities (a-c) and turbulent kinetic energy in three directions (d-f). $\delta^+/d^+ = 1/3$.

5 Correlation Between the Wake and the Oncoming Flow

In this section, the interaction between the wake and the oncoming flow are examined, and their correlation is analyzed. In order to reveal the unsteady features of the wake in response to the oncoming flow, time-dependent velocity fluctuations of the wake and the oncoming flow in three directions are monitored. In addition, spectral features are also investigated to ensure the correlation between the wake and the oncoming flow.

5.1 Time-Dependent Response of the Wake to the Oncoming Fluctuation

The flow velocity fluctuations at four monitoring points behind each sphere are investigated. These points are 1.0d, 3.0d, 5.0d and 8.0d behind the sphere center, respectively. At the same time, the fluctuating velocities of the “undisturbed flow field”, in which the “reference sphere” is absent while the rough bed is still included, are also recorded (this required three additional simulations). The monitoring point in the undisturbed flow field is the location of the sphere center in the disturbed flow field. Data from this point can be regarded as the oncoming flow fluctuations seen by the reference particle. Because the fluid at different monitoring points responds at different time instants to the oncoming fluctuation (e.g. the fluid at 1.0d behind the sphere reacts earlier than that at 3.0d behind the sphere), the lines of the fluctuating velocities in the disturbed field are shifted along the horizontal axis properly in order to compare them clearly. The value of the shift varies with the location of the monitoring point, but basically it is the time

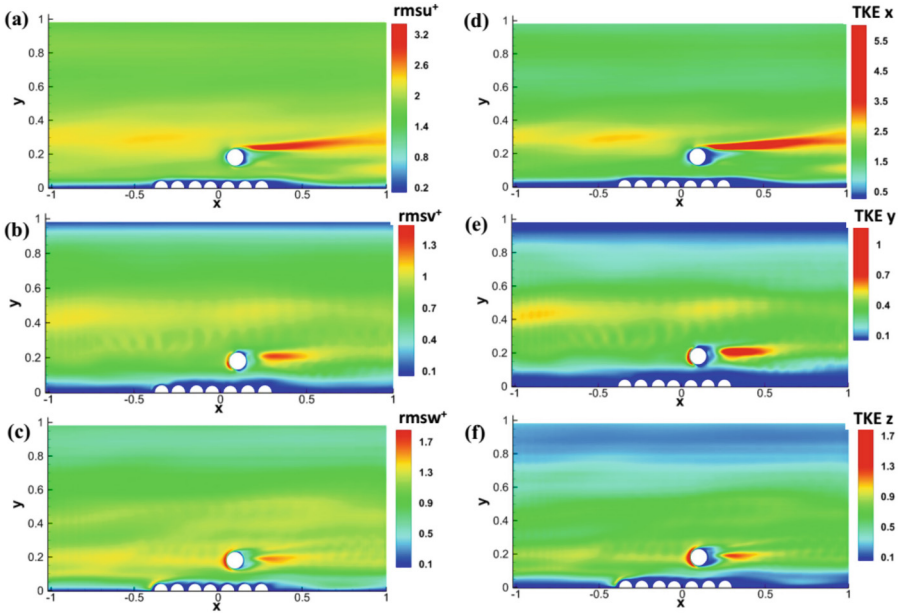


Fig. 10. Root mean square velocities (a-c) and turbulent kinetic energy in three directions (d-f). $\delta^+/d^+ = 1.0$.

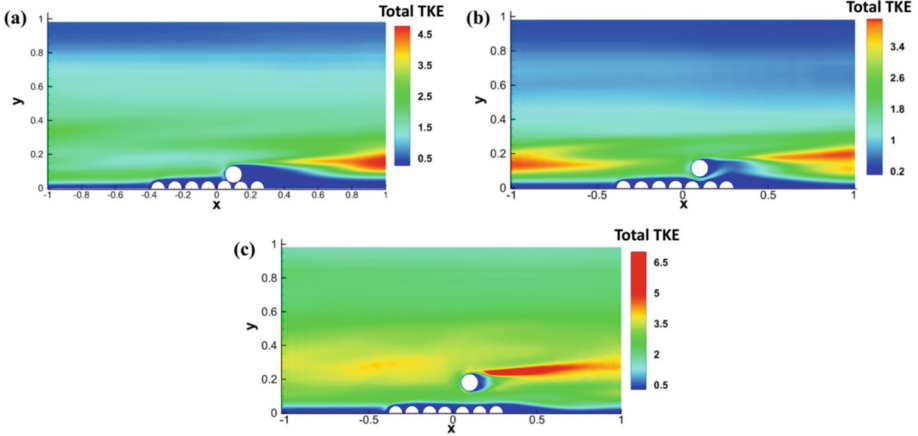


Fig. 11. Total turbulent kinetic energy on x-y plane. (a) $\delta^+/d^+ = 0.0$. (b) $\delta^+/d^+ = 1/3$. (c) $\delta^+/d^+ = 1.0$.

duration for a fluid parcel to flow from the sphere center to the streamwise location of the monitoring point. For example, for the monitoring point 8.0d behind the sphere center in Fig. 14, the shift value is about $t^+ = 13.0$. The results are shown in Fig. 12, 13 and 14.

Figure 12(a-c) shows the instantaneous fluctuating velocities of the four monitoring points behind the sphere of $\delta^+/d^+ = 0.0$, compared with that in the undisturbed flow. For this sphere, the wall-normal location of these monitoring points is at $y = 0.08165$ or $y^+ = 14.7$, the same as that of the sphere center. The first phenomenon we notice is that the wake fluctuation is inhibited near the sphere and becomes stronger downstream, which is in accordance with what is noticed in Fig. 8. Second, the fluctuation in the streamwise direction is larger than those in the other two directions. And, the wall-normal fluctuation is weaker than the spanwise one. This is also in agreement with the observations of Fig. 8. Third and most importantly, there is a correlation between the wake fluctuations and the oncoming ones. In Fig. 12(a), the wake fluctuation basically follows the oncoming one, though the magnitude is different. In comparison, the wall-normal and spanwise fluctuations show weaker correlations, as shown in Fig. 12(b) and 12(c), respectively. It should be noted in Fig. 12(a) the wake fluctuation in the vicinity of the sphere (1.0d behind the sphere) does not correlate with the oncoming flow.

For the case of $\delta^+/d^+ = 0.0$, the region of the largest turbulent kinetic energy in the wake is not located behind the sphere center, but above the four monitoring points. Therefore, the point above the fourth monitoring point (8.0d behind the sphere center) is also examined. This point is located at $y = 0.13165$ or $y^+ = 23.7$, the same vertical location as the sphere top. Thus, this point is referred to as the point behind the sphere top. In Fig. 12(d-f), the fluctuating velocities at the point 8.0d behind the sphere top is examined, compared with the oncoming fluctuations. Figure 12(d) shows the streamwise fluctuating velocities in the wake and the oncoming flow are in stronger correlation than those in Fig. 12(a). On the other hand, the wall-normal and spanwise wake fluctuations are not in such strong correlation with the oncoming velocity, as shown in Fig. 12(e) and 12(f), respectively.

For the sphere of $\delta^+/d^+ = 1/3$ shown in Fig. 13, the wake and oncoming fluctuation in the streamwise direction are in very weak correlation, which is the case for both the monitoring points behind the sphere center and that behind the sphere top. However, in the wall-normal direction, except the point very near the sphere (which locates 1.0d behind the sphere center), the correlation is stronger, especially between the wake fluctuation 8.0d behind the sphere top and the oncoming one (Fig. 13e). Though the fluctuating magnitudes are not always the same, the fluctuating directions are similar. It means the sphere amplifies or inhibits the oncoming disturbance. In the spanwise direction, the correlation is even stronger. In Fig. 13(c), it can be noticed these profiles show a very similar trend, tending to collapse onto each other. This phenomenon can also be noticed in Fig. 13(f). In addition, the turbulence augmentation exists in the wall-normal and spanwise directions, but not in the streamwise direction.

For the sphere of $\delta^+/d^+ = 1.0$ shown in Fig. 14(a), the wake fluctuation behind the sphere center and oncoming fluctuation in the streamwise direction are in weak correlation, but these monitoring points lie outside the streamwise turbulence augmentation region shown in Fig. 10(a) and 10(d). On the other hand, the wake fluctuation at 1.0d behind the sphere top shows a strong correlation with the oncoming one, as shown in Fig. 14(d). In the wall-normal direction shown in Fig. 14(b), the correlation between the oncoming fluctuation and the wake fluctuations directly behind the sphere center is much stronger, even for the point 1.0d behind the sphere. In addition, the largest fluctuation

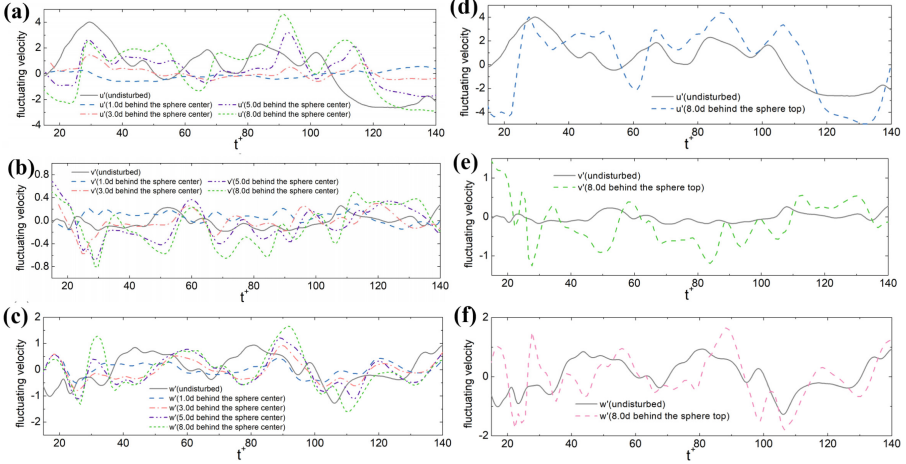


Fig. 12. Time-dependent fluctuating velocities of in the streamwise, wall-normal and spanwise directions of the sphere of $\delta^+/d^+ = 0.0$. (a-c): Time-dependent fluctuating velocities behind the sphere center ($y^+ = 14.7$). (d-f): Time-dependent fluctuating velocities behind the sphere top ($y^+ = 23.7$). (a, d): Streamwise fluctuating velocities. (b, e): Wall-normal fluctuating velocities. (c, f): Spanwise fluctuating velocities. Because the fluid at different monitoring points responds at different time instants to the oncoming fluctuation (e.g. the fluid at $1.0d$ behind the sphere reacts earlier than that at $3.0d$ behind the sphere), the lines of the fluctuating velocities in the disturbed field are shifted along the horizontal axis (time axis) properly in order to be shown more clearly.

magnitude lies at the second monitoring point ($3.0d$ behind the sphere), unlike the other two cases ($\delta^+/d^+ = 0.0$ and $\delta^+/d^+ = 1/3$). This is in accordance with turbulence augmentation region shown in Fig. 10(b) and 10(e). A strong correlation also exists in the spanwise direction, except the point $1.0d$ behind the sphere, as shown in Fig. 14(c).

5.2 Spectral Features of the Wake and the Oncoming Flow

In order to investigate the spectral features of the wake and its relation to the oncoming flow, we analyze the amplitudes of the wake fluctuation and the oncoming fluctuation in the frequency domain. Figure 15 shows the spectra of the case of $\delta^+/d^+ = 0.0$. Fig. 15(a) shows the wake to be in strong correlation with the oncoming flow and the amplitude of the fluctuation in the wake to be generally larger than that of the oncoming flow, indicating that the oncoming fluctuation is amplified in the wake in the streamwise direction. It is interesting that the amplification ratios at different frequencies are different. However, in the other two directions shown in Fig. 15(b) and 15(c), the correlation is relatively weak, and the amplitude is not amplified.

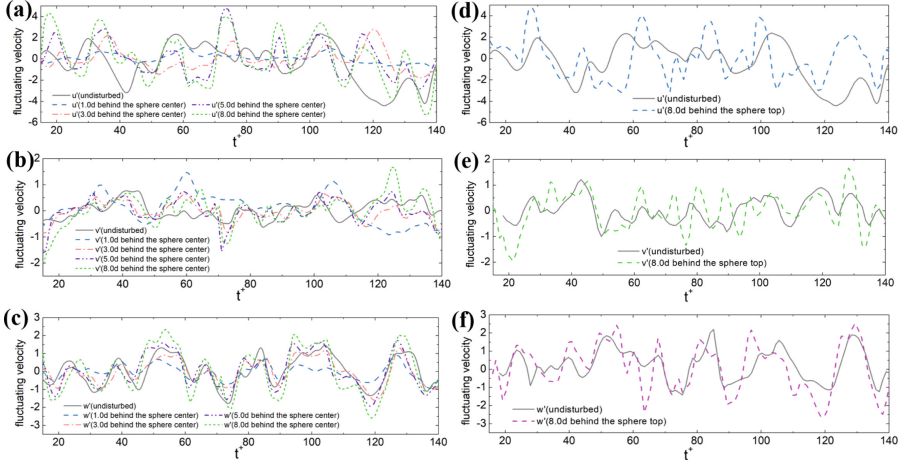


Fig. 13. Time-dependent fluctuating velocities of in the streamwise, wall-normal and spanwise directions of the sphere of $\delta^+/d^+ = 1/3$. (a-c): Time-dependent fluctuating velocities behind the sphere center ($y^+ = 20.7$). (d-f): Time-dependent fluctuating velocities behind the sphere top ($y^+ = 29.7$). (a, d): Streamwise fluctuating velocity. (b, e): Wall-normal fluctuating velocity. (c, f) Spanwise fluctuating velocity. The lines of the fluctuating velocities in the disturbed field are shifted along the horizontal axis (time axis) properly in order to be shown more clearly.

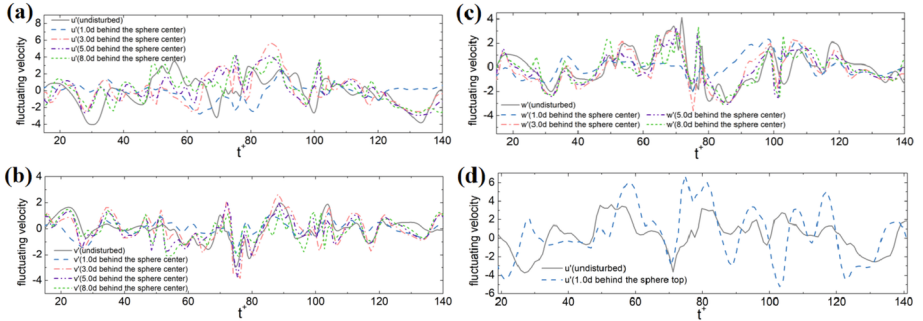


Fig. 14. Time-dependent fluctuating velocities of in the streamwise, wall-normal and spanwise directions of the sphere of $\delta^+/d^+ = 1.0$. (a-c): Time-dependent fluctuating velocities behind the sphere center ($y^+ = 23.7$). (d): Time-dependent streamwise fluctuating velocity behind the sphere top ($y^+ = 41.7$). The lines of the fluctuating velocities in the disturbed field are shifted along the horizontal axis (time axis) properly in order to be shown more clearly.

Figure 16 shows the case of $\delta^+/d^+ = 1/3$. In this case, wake fluctuations in all three directions are correlated with the oncoming ones. In addition, nearly all three components of wake fluctuations are larger than those in the oncoming flow. For the case of $\delta^+/d^+ = 0.0$, the wake of the sphere is greatly affected by the wall, and the viscous effect plays a very important role. Thus, the wake fluctuations are not so large. However, for the case of $\delta^+/d^+ = 1/3$, Re_p increases to a range of $157 \sim 280$, and the wake fluctuations increase rapidly. Meanwhile, the fluctuations in the oncoming flow,

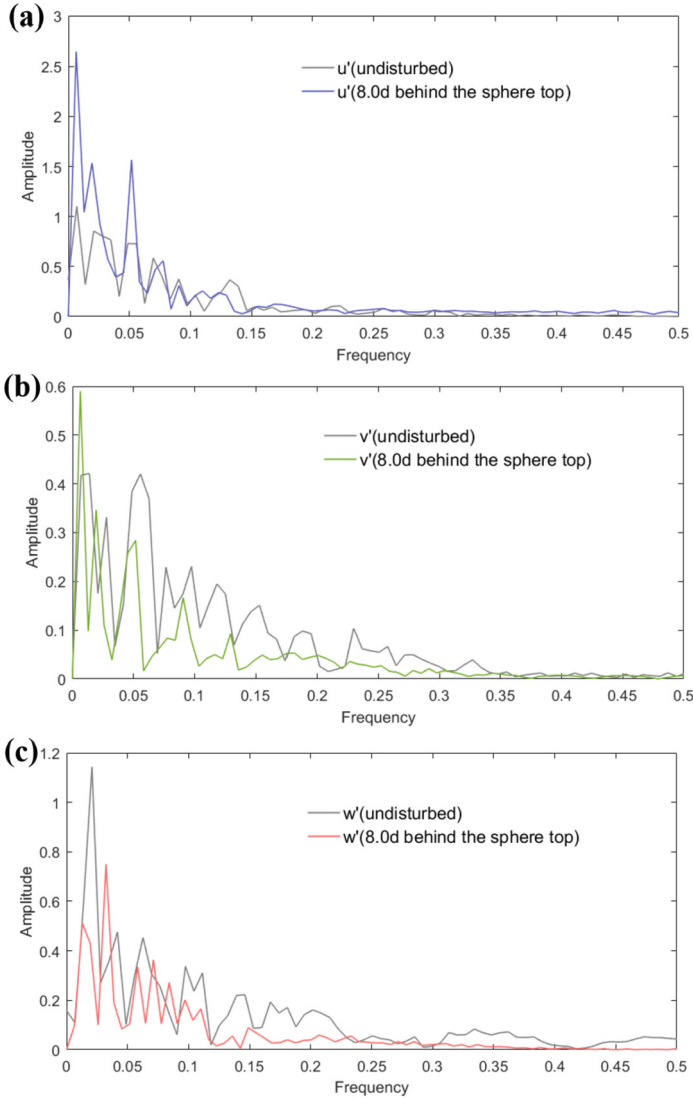


Fig. 15. Spectra of the wake fluctuations compared with those of the oncoming fluctuations for the case of $\delta^+/d^+ = 0.0$. (a) Streamwise direction; (b) Wall-normal direction; (c) Spanwise direction.

though increases slightly, still remain at low levels, especially in the wall-normal and spanwise directions. This is the reason why wake fluctuations are larger than those in the oncoming ones. As δ^+/d^+ increases to 1.0, the oncoming fluctuations experienced by the sphere increase to nearly the largest in the channel, so the wake fluctuations are not that large in comparison. This difference in the behavior of the intermediate separation case is consistent with the earlier observations. This also reveals the interesting fact that the

back effect of the particle on the ambient turbulence is not monotonically dependent on either the gap between the particle and the wall or correspondingly the particle Reynolds number.

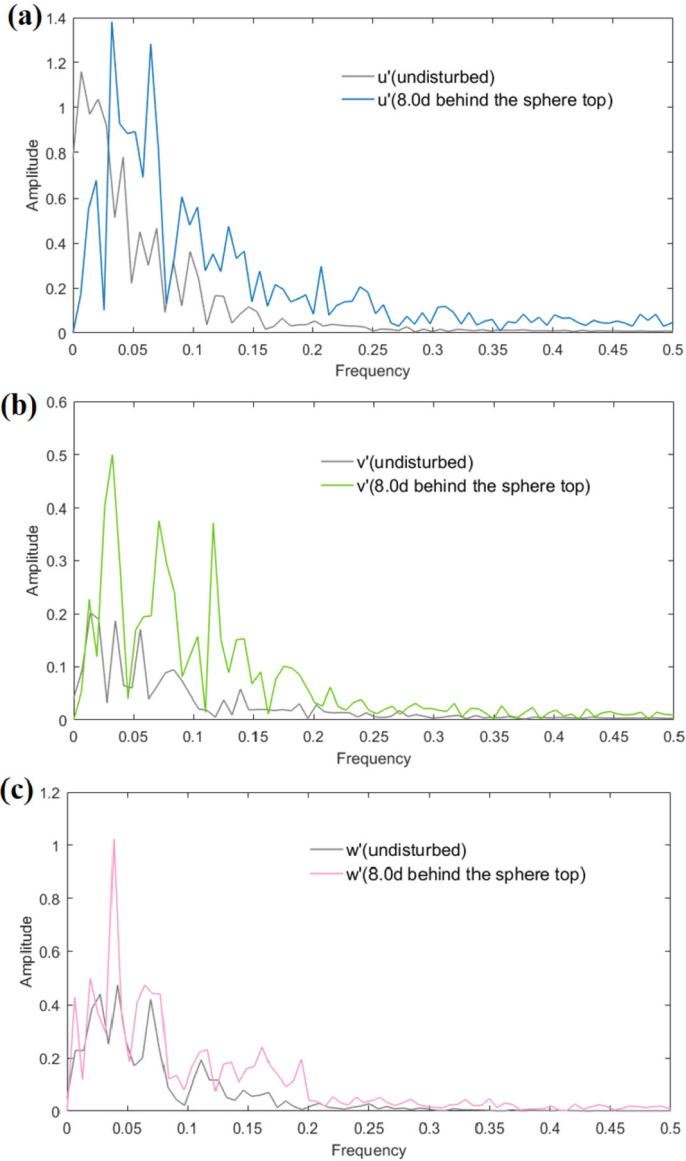


Fig. 16. Spectra of the wake fluctuations compared with those of the oncoming fluctuations for the case of $\delta^+/d^+ = 1/3$. (a) Streamwise direction; (b) Wall-normal direction; (c) Spanwise direction.

The case of $\delta^+/d^+ = 1.0$ is shown in Fig. 17. Like the previous case, strong correlations are noticed in all three components. Besides that, the most important observation is that a peak can be seen at about $f = 2.0$, both in Fig. 17(a) and 17(b). The peak is obviously taller than those near it. The height of this peak is apparently larger than that of the oncoming flow at $f = 2.0$, and the amplification ratio at this frequency is the largest. It is inferred this frequency is at which the natural vortex shedding happens. Thus, it could be inferred that the force on the particle may be mostly affected by the wake at the

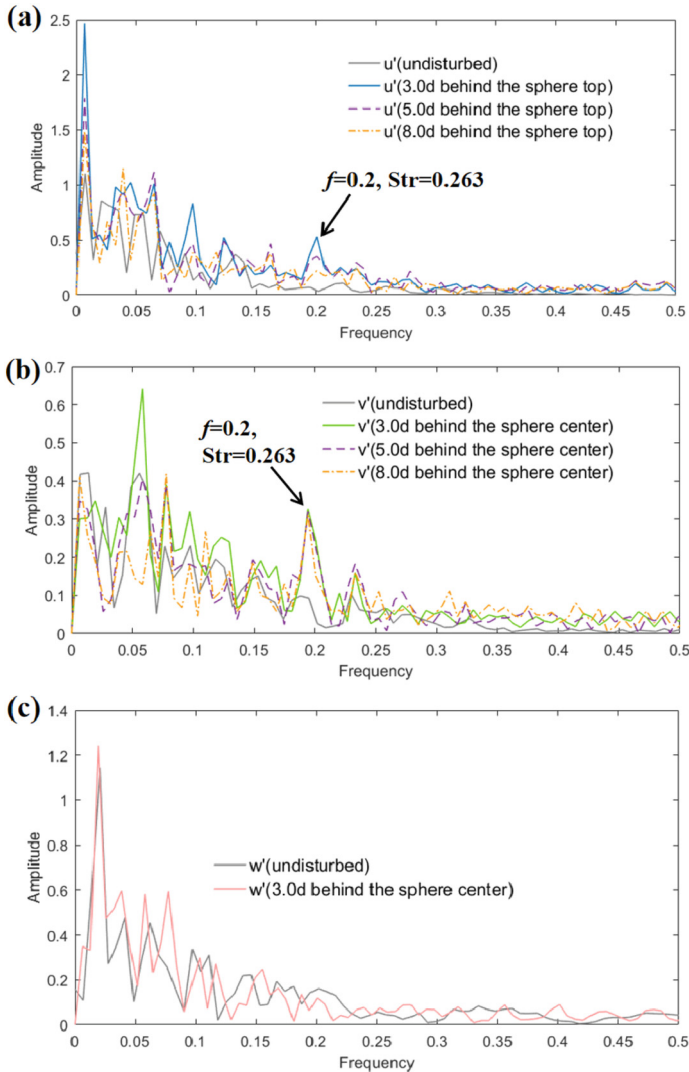


Fig. 17. Spectra of the wake fluctuations compared with those of the oncoming fluctuations for the case of $\delta^+/d^+ = 1.0$. (a) Streamwise direction; (b) Wall-normal direction; (c) Spanwise direction.

natural vortex shedding frequency. The Strouhal number (based on the particle center velocity) at $f = 2.0$ is 0.263, about twice of that of the vortex shedding behind a sphere in isotropic turbulence. Zeng et al. [25] investigated finite-sized particles in wall turbulence and found that the Strouhal number of dominant vortex shedding to be from 0.103 to 0.138 and to be in agreement with that in isotropic turbulence reported in Bagchi and Balachandar [41]. But, a peak at Strouhal number of 0.203 was also noticed, and this could be the Strouhal number of natural vortex shedding. Steward et al. [21] and Rao et al. [22] investigated the wake of a rolling sphere in a wall-bounded laminar flow and the Strouhal number was found to be around 0.12, which is close to the Strouhal number in an unbounded flow obtained by Tomboulides & Orszag [9] and Johnson & Patel [7].

6 Discussion

6.1 Correlation between the Wake and the Oncoming Flow

Our simulations show that a strong correlation between the wake fluctuation and the oncoming one exists in many cases. The oncoming fluctuation induces the shedding of vortices and the wake oscillates in the same direction as the oncoming fluctuation. This gives us the hope to establish a deterministic model for the wake-induced force on the sphere, which are urgently needed for the closure of the large eddy simulation (LES) of particle-laden flows. Nevertheless, some difficulties still exist. For example, the magnitude of wake fluctuation is quite different from the oncoming one, so the extent of force alteration by the wake is still unknown. In addition, the natural vortex shedding is found to be important in the case of $\delta^+/d^+ = 1.0$, but the relative contribution of shedding to overall force fluctuation is unclear.

A deterministic instantaneous turbulence modulation model for the wake may also be possible. The wake oscillation is dictated by the oncoming flow. Thus, the prediction of the instantaneous wake oscillation may be possible if the oncoming turbulence is resolved and the flow is moderately turbulent. The correlation is closely related to turbulence modulation. The region of turbulence augmentation is less affected by the viscous effect and is controlled mainly by the oncoming flow, and thus the correlation between turbulence augmentation region in the wake and the oncoming flow is strong. Therefore, strong correlation arises with the turbulence augmentation in the wake. On the other hand, as discussed in Sect. 6.1, the near-wall region is mainly affected by the viscous effect of the rough bed and turbulence attenuation follows. It is less affected by the oncoming flow and thus is where the correlation between the oncoming flow and the wake is weak.

6.2 Turbulence Modulation by the Wake

Turbulence modulation by the sphere wake is understandably depends on the location of the sphere due to the inhomogeneity and anisotropy of the wall-bounded flow. The region of turbulence augmentation is dictated by both the location with respect to the sphere and the sphere's location with respect to the rough wall. Basically, turbulence attenuation arises due to the strong viscous effect near the sphere surface and the wall.

Away from the sphere and the wall, turbulence augmentation is notable, especially on the upper side of the sphere. Due to the presence of the wall, vortex shedding on the lower side of the sphere is inhibited, and it is much more notable on the upper side of the sphere. At relatively low particle Reynolds number, which are the cases of $\delta^+/d^+ = 0.0$ and $\delta^+/d^+ = 1/3$, turbulence augmentation exists far downstream, even at distances more than ten times of the sphere diameter, indicating that the influence of the wake is profound and definitely not just limited to regions near the sphere, which was also suggested by Zeng et al. [28]. As the particle Reynolds number increases, the vortices are shed more rapidly, and the region of turbulence augmentation is much closer to the sphere, which is the case for $\delta^+/d^+ = 1.0$. Compared to turbulence attenuation around the particle reported in [30] at lower Reynolds numbers of $Re_p = 27 \sim 126$, the higher Re_p in the present research causes an apparent turbulence augmentation. For the case of $\delta^+/d^+ = 1/3$, turbulence augmentation in the streamwise direction near the particle does not arise like the other two cases.

The results of a sphere above a rough-wall (the case of $\delta^+/d^+ = 1/3$) and above a smooth-wall (Case 4 in Zeng et al. [28]) can be compared. In Case 4 of Zeng et al. [28], the sphere diameter is $d^+ = 24.94$ and the gap between the sphere and the wall is $\delta^+ = 5.5$. The rough-wall and the smooth-wall cases share several similarities. The one-sided vortex shedding in both cases induces more intense turbulent fluctuations on the upper side of the sphere. A region of turbulence augmentation ahead of the sphere exists in both cases. And, the patterns of the turbulent modulation away from the wall are similar. The differences lie in the near-wall region. In the smooth-wall case, the turbulent fluctuation in the gap is extremely high, even reaches the highest level in the wall-normal and spanwise components. But it is not the case for the rough-wall. The rough wall creates a larger viscous-dominated region near the wall, and the turbulent fluctuations within the gap are much lower than those in a smooth-wall case (see Fig. 9). If the gap between the sphere and the wall is large enough (e.g. $\delta^+/d^+ = 1.0$), the effect of wall roughness is minimal.

6.3 Natural Vortex Shedding of a Sphere

In the present simulations, the sphere is stationary in a rough-wall-bounded turbulent flow. The Strouhal number in the simulation is about 0.263, which is in agreement with the experimental measurement over the range 0.26 to 0.33 [42]. It is about twice of the Strouhal number of vortex shedding of a sphere in an unbounded flow [7, 9] and a rolling sphere near a wall in a uniform flow [21, 22]. The vortex shedding on the lower side of the sphere is inhibited due to the presence of the wall, so the shedding only persists on the upper side. Thus, the flow on the upper side of the sphere plays a more important role in determining the vortex shedding frequency. Since the Strouhal number is still calculated based on the particle center velocity, the Strouhal number is larger than that of vortex shedding in an unbounded flow or a rolling sphere.

The role of natural vortex shedding in the presence of ambient turbulence is still ambiguous. It depends on the turbulent intensity, the particle Reynolds number, and the size of the oncoming vortex. In our case, the length scale of the oncoming vortex is of the same order of magnitude as that of the sphere, which may be the reason why the natural vortex shedding is dominated by the oncoming vortex structure. We conjecture if

the scale of the oncoming fluctuation is small enough, the natural vortex shedding may be prominent in the wake.

7 Concluding Remarks

In this paper, we performed direct numerical simulations with the immersed boundary method to investigate the interaction between the wake of a finite-sized sphere above a rough bed and the ambient wall-bounded turbulence. The flow is moderately turbulent at $Re_\tau = 180$. The sphere with the diameter of $d^+ = 18$ is placed in three vertical locations above the rough bed, which are $\delta^+/d^+ = 0.0$, $\delta^+/d^+ = 1/3$, and $\delta^+/d^+ = 1.0$, respectively. We focused on analyzing the time-dependent features of the turbulence/wake interaction and the turbulence modulation by the wake. The key findings are summarized as follows:

(1) The correlation between the velocity fluctuations in the sphere wake in regions of turbulence augmentation and the oncoming flow fluctuation is strong. The oncoming fluctuation induces the shedding of vortices and the wake oscillates in the same direction as the oncoming flow. The strongest correlation is found in the region of turbulence augmentation by the sphere wake. This phenomenon provides a possible way to build a deterministic model for the wake-induced force on the sphere, though further study is still needed for complete understanding. This kind of model can be beneficial for the closure of the large eddy simulation (LES) of particle-laden flows. In addition, a deterministic instantaneous turbulence modulation model for the wake is also possible based on this correlation.

(2) Turbulence attenuation region is found near the sphere and the wall due to the viscous effect. While the region of turbulence augmentation lies farther away from the wall and farther downstream. As the particle Reynolds number increases, the region of turbulence augmentation becomes closer to the sphere. For the case of $\delta^+/d^+ = 1/3$, the turbulence augmentation in the streamwise direction is not observed.

(3) The rough wall induces a larger viscous-dominated region than the smooth wall. Thus, the turbulence fluctuation in the gap between the sphere and the wall is weaker than that in the smooth-wall cases. Basically, the effect of roughness is prominent in the near-wall region. If the gap is large enough, the roughness plays a minimal role.

(4) Due to the presence of the wall, the vortex shedding happens on only one side of the sphere (upper side). The Strouhal number of the natural vortex shedding based on the particle center velocity is around 0.262, about twice that in an unbounded flow. This difference is partly due to the normalization by the velocity at the center of the particle while shedding mostly occurs only at the high-speed size on the top side of the particle. In the cases studied here, the natural vortex shedding is overwhelmed by the ambient turbulence. However, the natural vortex shedding can be prominent when the largest eddy of the ambient turbulence is smaller than the shedding vortices. Further study is still needed on that issue.

8 Statements and Declarations

The authors declare that they have no known competing financial interests or personal relationships that could have appeared to influence the work reported in this paper.

Acknowledgements. X.L. acknowledges the financial support from China Scholarship Council (CSC). This research is also supported by the Project funded by China Postdoctoral Science Foundation (No. 2020M683473).

References

1. Mathai, V., Prakash, V.N., Brons, J., Sun, C., Lohse, D.: Wake-driven dynamics of finite-sized buoyant spheres in turbulence. *Phys. Rev. Lett.* **115**(12), 124501 (2015)
2. Wu, J.S., Faeth, G.M.: Sphere wakes in still surroundings at intermediate Reynolds numbers. *AIAA J.* **31**(8), 1448–1455 (1993)
3. Leweke, T., Provansal, M., Ormières, D., Lebescond, R.: Vortex dynamics in the wake of a sphere. *Phys. Fluids* **11**(9), S12 (1999)
4. Chrust, M., Goujon-Durand, S., Wesfreid, J.E.: Loss of a fixed plane of symmetry in the wake of a sphere. *J. Fluids Struct.* **41**, 51–56 (2013)
5. Ern, P., Risso, F., Fabre, D., Magnaudet, J.: Wake-induced oscillatory paths of bodies freely rising or falling in fluids. *Annu. Rev. Fluid Mech.* **44**(1), 97–121 (2012)
6. Natarajan, R., Acrivos, A.: The instability of the steady flow past spheres and disks. *J. Fluid Mech.* **254**, 323–344 (1993)
7. Johnson, T.A., Patel, V.C.: Flow past a sphere up to a Reynolds number of 300. *J. Fluid Mech.* **378**, 19–70 (2000)
8. Ghidersa, B., Dušek, J.: Breaking of axisymmetry and onset of unsteadiness in the wake of a sphere. *J. Fluid Mech.* **423**, 33–69 (2000)
9. Tomboulides, A.G., Orszag, S.A.: Numerical investigation of transitional and weak turbulent flow past a sphere. *J. Fluid Mech.* **416**, 45–73 (2000)
10. Eshbal, L., Rinsky, V., David, T., Greenblatt, D., van Hout, R.: Measurement of vortex shedding in the wake of a sphere at $Re=465$. *J. Fluid Mech.* **870**, 290–315 (2019)
11. Eshbal, L., Kovalev, D., Rinsky, V., Greenblatt, D., van Hout, R.: Tomo-PIV measurements in the wake of a tethered sphere undergoing VIV. *J. Fluids Struct.* **89**, 132–141 (2019)
12. Citro, V., Siconolfi, L., Fabre, D., Giannetti, F., Luchini, P.: Stability and sensitivity analysis of the secondary instability in the sphere wake. *AIAA J.* **55**(11), 3661–3668 (2017)
13. Kim, H.J., Durbin, P.A.: Observations of the frequencies in a sphere wake and of drag increase by acoustic excitation. *Phys. Fluids* **31**(11), 3260–3265 (1988)
14. Sakamoto, H., Haniu, H.: A study on the vortex shedding from spheres in a uniform flow. *Trans. ASME J. Fluids Engng.* **112**, 386–392 (1990)
15. Ploumhans, P., Winckelmans, G.S., Salmon, J.K., Leonard, A., Warren, M.S.: Vortex methods for direct numerical simulation of three-dimensional bluff body flows: application to the sphere at $Re=300$, 500, and 1000. *J. Comput. Phys.* **178**(2), 427–463 (2002)
16. Yun, G., Kim, D., Choi, H.: Vortical structures behind a sphere at subcritical Reynolds numbers. *Phys. Fluids* **18**(1), 015102 (2006)
17. Terra, W., Sciacchitano, A., Scarano, F.: Aerodynamic drag of a transiting sphere by large-scale tomographic-PIV. *Exp. Fluids* **58**(7), 83 (2017)
18. David, T., Eshbal, L., Rinsky, V., van Hout, R.: Flow measurements in the near wake of a smooth sphere and one mimicking a pine cone. *Phys. Rev. Fluids.* **5**(7), 074301 (2020)
19. Zeng, L., Balachandar, S., Fischer, P.: Wall-induced forces on a rigid sphere at finite Reynolds number. *J. Fluid Mech.* **536**, 1–25 (2005)
20. Zeng, L., Najjar, F., Balachandar, S., Fischer, P.: Forces on a finite-sized particle located close to a wall in a linear shear flow. *Phys. Fluids* **21**(3), 033302 (2009)
21. Stewart, B.E., Thompson, C.M., Leweke, T., Hourigan, K.: Numerical and experimental studies of the rolling sphere wake. *J. Fluid Mech.* **643**(4), 137–162 (2010)

22. Rao, A., Passaggia, P.Y., Bolnot, H., Thompson, M.C., Leweke, T., Hourigan, K.: Transition to chaos in the wake of a rolling sphere. *J. Fluid Mech.* **695**, 135–148 (2012)
23. Mittal, R.: Response of the sphere wake to free-stream fluctuations. *Theor. Comput. Fluid Dyn.* **13**, 397–419 (2000)
24. Bagchi, P., Balachandar, S.: Response of the wake of an isolated particle to isotropic turbulent cross-flow. *J. Fluid Mech.* **518**, 95–123 (2004)
25. Zeng, L., Balachandar, S., Najjar, F., Fischer, P.: Interaction of a finite-sized particle with wall turbulence. *J. Fluid Mech.* **594**, 201–205 (2008)
26. Balachandar, S., Eaton, J.K.: Turbulent dispersed multiphase flow. *Annu. Rev. Fluid Mech.* **42**(1), 111–133 (2010)
27. Wu, J.S., Faeth, G.M.: Effect of ambient turbulence intensity on sphere wakes at intermediate Reynolds number. *AIAA J.* **33**(1), 171–173 (1995)
28. Zeng, L., Balachandar, S., Najjar, F.: Wake response of a stationary finite-sized particle in a turbulent channel flow. *Intl. J. Multiphase Flow* **36**(5), 406–422 (2010)
29. Naso, A., Prosperetti, A.: The interaction between a solid particle and a turbulent flow. *New J. Phys.* **12**(3), 033040 (2010)
30. Cisse, M., Homann, H., Bec, J.: Slipping motion of large neutrally buoyant particles in turbulence. *J. Fluid Mech.* **735**, R1 (2013)
31. van Hout, R., Eisma, J., Elsinga, G.E., Westerweel, J.: Experimental study of the flow in the wake of a stationary sphere immersed in a turbulent boundary layer. *Phys. Rev. Fluids.* **3**(2), 024601 (2018)
32. Xu, H., Bodenschatz, E.: Motion of inertial particles with size larger than Kolmogorov scale in turbulent flows. *Physica D* **237**, 14–17 (2008)
33. Bellani, G., Byron, M.L., Collignon, A.G., Meyer, C.R., Variano, E.A.: Shape effects on turbulent modulation by large nearly neutrally buoyant particles. *J. Fluid Mech.* **712**, 41–60 (2012)
34. Bellani, G., Nole, M.A., Variano, E.A.: Turbulence modulation by large ellipsoidal particles: concentration effects. *Acta Mech.* **224**(10), 2291–2299 (2013)
35. Yu, W., Vinkovic, I., Buffat, M.: Acceleration statistics of finite-size particles in turbulent channel flow in the absence of gravity. *Flow Turb. Combust.* **96**(1), 183–205 (2015)
36. Li, X., Balachandar, S., Lee, H., Bai, B.: Fully resolved simulations of a stationary finite-sized particle in wall turbulence over a rough bed. *Phys. Rev. Fluids.* **4**(9), 094302 (2019)
37. Lee, H., Balachandar, S.: Effects of wall roughness on drag and lift forces of a particle at finite Reynolds number. *Intl. J. Multiphase Flow.* **88**, 116–132 (2017)
38. Uhlmann, M.: An immersed boundary method with direct forcing for the simulation of particulate flows. *J. Comput. Phys.* **209**(2), 448–476 (2005)
39. Lee, H., Balachandar, S.: Critical shear stress for incipient motion of a particle on a rough bed. *J. Geophys. Res. Earth Surf.* **117**, F01026 (2012)
40. Lee, H., Ha, M.Y., Balachandar, S.: Work-based criterion for particle motion and implication for turbulent bed-load transport. *Phys. Fluids* **24**(11), 116604 (2012)
41. Bagchi, P., Balachandar, S.: Effect of turbulence on the drag and lift of a particle. *Phys. Fluids* **15**(11), 3496–3513 (2003)
42. Li, X., Bai, B.: Wake of a stationary sphere near a wall. *CIESC J.* **70**(9), 3300–3306 (2019)